Search for neutron excitations across the $N = 20$ shell gap in $^{25-29}$Ne

M. Belleguic,[1] F. Azaiez,[1] Zs. Dombrádi,[2] D. Sohler,[2] M. J. Lopez-Jimenez,[3] T. Otsuka,[4] M. G. Saint-Laurent,[3] O. Sorlin,[1] M. Stanoiu,[1,3] Y. Utsuno,[5] Yu.-E. Penionzhkevich,[6] N. L. Achouri,[7] J. C. Angelique,[7] C. Borcea,[8] C. Bourgeois,[1] J. M. Daugas,[3] F. De Oliveira-Santos,[3] Z. Dlouhy,[9] C. Donzaud,[1] J. Duprat,[1] Z. Elekes,[2] S. Grévy,[7] D. Guillemaud-Mueller,[1] S. Leenhardt,[1] M. Lewitowicz,[3] S. M. Lukyanov,[6] W. Mittig,[3] M. G. Porquet,[10] F. Pougheon,[1] P. Roussel-Chomaz,[3] H. Savajols,[3] Y. Sobolev,[6] C. Stodel,[3] and J. Timár[2]

[1]*Institut de Physique Nucléaire, IN2P3-CNRS, F-91406 Orsay Cedex, France*
[2]*Institute of Nuclear Research of the Hungarian Academy of Sciences, P.O. Box 51, Debrecen, H-4001, Hungary*
[3]*GANIL, B. P. 55027, F-14076 Caen Cedex 5, France*
[4]*Department of Physics, University of Tokyo, Hongo, Tokyo 113-0033, Japan*
[5]*Japan Atomic Energy Research Institute, Tokai, Ibaraki 319-0033, Japan*
[6]*FLNR, JINR, Ru-141980 Dubna, Moscow region, Russia*
[7]*Laboratoire de Physique Corpusculaire, 14000 Caen Cedex, France Caen F-14021, France*
[8]*IFIN-HH, P. O. Box MG-6, R-76900 Bucharest-Magurele, Romania*
[9]*Nuclear Physics Institute, AS CR, CZ 25068, Rez, Czech Republic*
[10]*CSNSM, IN2P3-CNRS and Université Paris-Sud, F-91405 Orsay Campus, France*

(Received 27 October 2004; revised manuscript received 30 June 2005; published 22 November 2005)

Nuclear structure of the neutron rich $^{25-29}$Ne nuclei has been investigated through the in-beam γ-ray spectroscopy technique using fragmentation reactions of both stable and radioactive beams. Level schemes have been deduced for these Ne isotopes. In order to examine the importance of intruder *fp* configurations, they are compared to shell model calculations performed either in the restricted *sd* or in the larger *sdpf* valence space. The ^{25,26}Ne and ^{27}Ne nuclei were found to be in agreement with the *sd* shell model calculations, whereas ^{28}Ne exhibits signatures of the intruder *fp* shell contribution.

DOI: 10.1103/PhysRevC.72.054316 PACS number(s): 23.20.Lv, 25.70.Mn, 27.30.+t, 21.60.Cs

I. INTRODUCTION

The breaking of the $N = 20$ shell closure far from stability was first evidenced in the ^{32}Mg nucleus [1]. The divergence between shell model calculations in the *sd* shells and observed properties of neutron-rich Ne, Na, and Mg isotopes [1–4] was ascribed to the inversion of the spherical closed-shell configurations and the deformed multiparticle-multihole (ph) intruder configurations. This phenomenon appears in a rather limited area of the nuclear chart, the so-called island of inversion, where nuclei gain in correlation energy through *ph* excitations across the $N = 20$ shell gap. Several theoretical calculations were accomplished to understand the structure of nuclei in this region and to estimate the relative energies between the normal and intruder configurations [5–9]. All these models predict that the intruder configuration takes over at $N \geqslant 20$ whereas it lies at an excitation energy ranging from 1.8 to 3.0 MeV at $N = 18$.

Calculations in the full neutron valence space consisting of the *sd*-shell plus the $f_{7/2}$ and $p_{3/2}$ orbits were performed in Ref. [10] using the Monte Carlo shell model (MCSM). As discussed in Ref. [11], the monopole component of their effective interaction differs from that used in other models. As a result, MCSM calculations predict an enhancement of the intruder mixing, reducing the $d_{3/2}$-$f_{7/2}$ neutron shell-gap at ^{28}O to 1.2 MeV, as compared to 5 MeV in the *sd* shell model calculation in Ref. [5]. Consequently MCSM calculations widen the island of inversion at lighter elements, which seems to be supported by experimental observations. The high level density observed at low excitation energy, e.g., in ^{31}Mg [2] or ^{29}Ne [3] are clear indications of the influence of intruder states at low excitation energy at $N = 19$. In addition, the low energy of the 2_1^+ states in the $N = 18$ nuclei of ^{30}Mg [1] and especially ^{28}Ne [4] may also be considered as signatures of a structural change, which may arise as a consequence of mixing of normal and intruder configurations [10]. The present article concerns the study of the structure of neutron rich ^{26,28}Ne isotopes, aiming for the search of intruder states. In addition, experimental results on neighbouring odd Ne isotopes are also presented.

II. EXPERIMENTAL METHOD

In order to obtain information on the structure of neutron rich Neon isotopes, in-beam γ-ray spectroscopy using the projectile fragmentation reactions has been used [4,12,13]. This method was applied to study neutron-rich nuclei in the vicinity of the $N = 28$ shell closure (e.g., ^{40,42,44}S [14], ^{43,45}Cl [15], and ^{45,46}Ar [16]) via fragmentation of a ^{48}Ca beam. The fragmentation of secondary beams produced by fragmentation of a ^{36}S beam was used to obtain information on the subshell closures at $N = 14,16$ [17].

Two experiments using the fragmentation of ^{36}S stable beam have been performed at GANIL. Both experiments are based on coincidence measurements between the projectile like fragments and their prompt γ-decay. A common γ-detector array has been used in both experiments. It consists of 74 BaF_2 detectors placed at a mean distance of 30 cm from the target covering a major part of the solid angle around it.

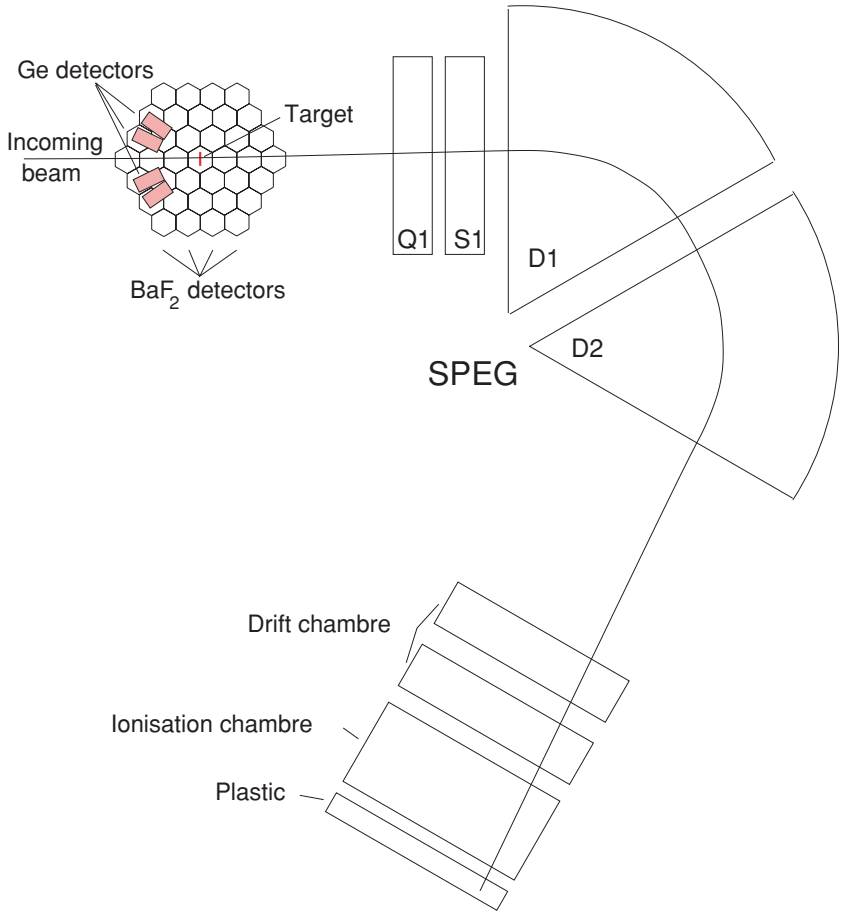

FIG. 1. (Color online) Schematic view of the experimental setup. Q1, S1, D1, D2 are the quadrupole, sextupole, and dipole magnets of the SPEG spectrograph.

The relatively high velocity of the produced projectile fragments ($v/c \simeq 0.35$) requires to apply proper Doppler shift corrections to the detected γ rays. The total photopeak efficiency of the BaF_2 array was found to be 30% for a typical γ-ray line at 1.3 MeV with an average FWHM of 12% after Doppler correction.

The first experiment consisted of using the fragmentation of a 77.5A MeV ^{36}S beam with an intensity of about 1 nA on a thin Be target (2.77 mg/cm^2) located at the entrance of SPEG, the energy loss spectrometer at GANIL. In addition to the BaF_2 array, four 70% high resolution Ge detectors were used at the most backward angles. The overall Ge detector efficiency was 0.12% at 1.3 MeV. In spite of having a low efficiency, the high resolution of the Ge detectors ($\sim$30 keV at 1.3 MeV after Doppler correction) helped a lot in the case of complex spectra. On the other hand, the relatively high efficiency of the BaF_2 array allows to perform γ-γ coincidences and help building level schemes. The schematic arrangement of the setup is shown in Fig. 1.

The produced fragments were selected and identified in the SPEG spectrometer [18] by the combined use of energy loss, total energy, time-of-flight, and focal-plane position information. This later parameter was used to correct the time-of-flight value from the various flight path lengths of the fragments in the spectrometer which was operated in a dispersive mode. The energy losses and positions of the fragments were determined by the use of an ionization (70 cm long) and a set of two x-y drift chambers (12 cm thick and 80 cm width each). Their residual energy was measured in a 2 cm thick plastic scintillator whose timing signal served to determine the time-of-flight (T_{pl}) of the fragments with respect to the cyclotron radio frequency. The spectrograph was optimized to $A/Z = \frac{8}{3}$ mass to charge ratio corresponding to ^{32}Mg. This value falls between ^{26}Ne and ^{27}Ne, but the isotope ^{28}Ne was also transmitted. The quality of the mass separation in the Ne isotopic chain is shown in Fig. 2. During

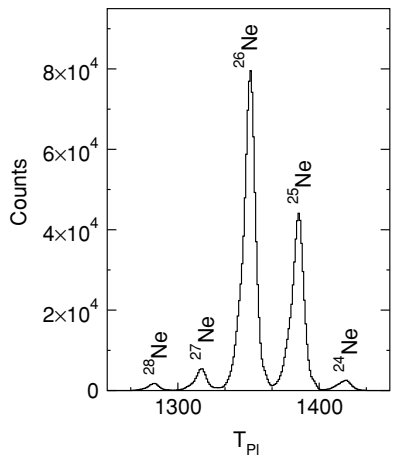

FIG. 2. Time-of-flight spectrum showing the amount of Ne isotopes produced in the present experiment.

the experiment we observed about 9×10^5 ^{26}Ne, 6×10^4 ^{27}Ne, and 2×10^4 ^{28}Ne nuclei. In the following this experiment will be refereed to as "single step fragmentation" experiment.

For the second experiment, we used a primary beam of ^{36}S delivered by the two GANIL cyclotrons at an energy of 77.5A MeV and an intensity of 400 pnA on a carbon target of 348 mg/cm^2 thickness placed in the SISSI device. The produced nuclei were selected through the ALPHA spectrometer using a 130 mg/cm^2 Al wedge. The magnetic rigidity of the ALPHA spectrometer and the optics of the beam line were optimized for the transmission of a secondary beam mainly composed of ^{24}F, ^{25,26}Ne, ^{27,28}Na, and ^{29,30}Mg fragments with energies varying from 54A MeV up to 65A MeV. An "active" target composed of a plastic scintillator (103 mg/cm^2) sandwiched by two carbon foils of 51 mg/cm^2 each was used at the same dispersive focus of SPEG as the Be target in the first experiment. The plastic scintillator part of the "active" target was used to identify the incoming nuclei on an event by event basis through energy loss and time of flight measurements. The fragments induced by reactions of the secondary beam are collected and identified at the SPEG spectrometer focal plane which was optimized for products with $A/Z = 3$. This method is called the "double step fragmentation" method because it uses two consecutive fragmentation reactions in order to populate the nuclei of interest. It is worth mentioning here that, mainly the Na and Mg component of the secondary beam cocktail populates the Ne fragments observed. In this experiment the BaF_2 detector thresholds were set to a minimum value of around 100 keV in order to allow the detection of the lowest γ-ray energies. In the single step reaction they were set to about 500 keV energy in the laboratory frame.

It is also worth to notice that in the case of a "single step fragmentation" the ^{36}S beam intensity has been limited to 6×10^9 pps in order to reduce the counting rate in the individual γ-ray detectors to a reasonable rate of 2×10^4 s^{-1}. This limits the use of this method to nuclei produced with cross sections of the order of $\sim$1 μbarn, or $\sim 10^{-6}$ part of the total cross section. In the case of "double step fragmentation" a secondary beam made of species closer to the nuclei of interest was used with an intensity of only 8×10^4 s^{-1}. With such a low secondary beam intensity, γ-ray spectroscopy of exotic nuclei produced with relatively high ($\sim$0.1 mb) cross sections was possible.

Regarding neutron emission from projectile-like and target-like fragments, in both experiments a careful time selection of the γ-rays emitted promptly in the collision is made. However, the prompt γ-peak in the time spectrum may contain some contribution from neutrons which would induce signals in the BaF_2 detectors. The high energy projectile-like neutrons are focused in the forward direction (below $\sim 40^\circ$), whereas those evaporated by the target-like zone are emitted isotropically. The time-of-flight difference between the high-energy neutrons and the γ-rays emitted from the target is too small to be distinguished with our detector resolution of about 2 ns. The BaF_2 detectors placed at forward angles recorded many signals induced by light charged particles and neutrons, consequently, these detectors were discarded from the analysis. Unfortunately, the other BaF_2 crystals also detected neutrons, which produced a continuous background in their spectra. Target-like evaporated neutrons exhibit a typical Maxwell-Boltzmann distribution peaked at about 2 MeV. The time-distribution in the BaF_2 crystals is a convolution between this distribution and the energy-dependent response function of the crystals. The high energy part of this distribution leaks into the prompt γ-peak. In addition, we have fast neutrons which were directly knocked out by the target nuclei from the projectile. These neutrons scatter to backward direction in the center of mass system, and cover a large angular range in the laboratory frame. Therefore, even with the cleanest cut made on the time spectrum to separate the γ-rays and neutron-induced signals some contribution of neutrons to the γ-ray spectrum remains. The neutrons induce (n, n') and $(n, n'\gamma)$ reactions in the various Ba isotopes of the BaF_2 crystals. This neutron-induced γ background in the BaF_2 detectors is smeared out in energy after summing all Doppler-corrected energies of individual crystals.

III. EXPERIMENTAL RESULTS

The γ-ray spectra obtained by use of the Ge detectors for ^{26,27}Ne in the single step fragmentation experiment are shown in Figs. 3 and 4, respectively. Those obtained by use of the BaF_2 detectors for ^{28}Ne in the single and double-step fragmentation experiments are shown in Figs. 5 and 6, respectively, whereas the spectrum for ^{29}Ne from the double-step fragmentation experiment is shown in Fig. 7. In addition, two transitions with energies of 1617(5) and 1707(4) keV have been observed in the germanium spectrum obtained for ^{25}Ne. These two transitions are in coincidence with each other, and in this way we confirm the results obtained on ^{25}Ne from β decay of ^{25}F [19]. In the spectrum obtained by the Ge detectors for ^{26}Ne, three high energy lines at 1499, 1671, and 2024 keV energies are clearly visible, the existence of which is supported also by the spectrum from the BaF_2 detectors. These γ-lines are assigned to ^{26}Ne. The 1671 and the 2024 keV γ-rays have already been

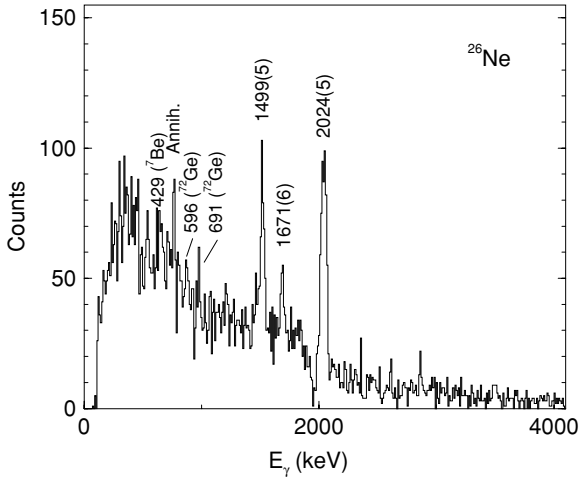

FIG. 3. Ge γ-ray spectrum of ^{26}Ne obtained by in-beam γ-spectroscopy using the fragmentation of a ^{36}S beam on a ^{9}Be target. The low energy peaks coming from target-like processes are shifted by the Doppler-correction.

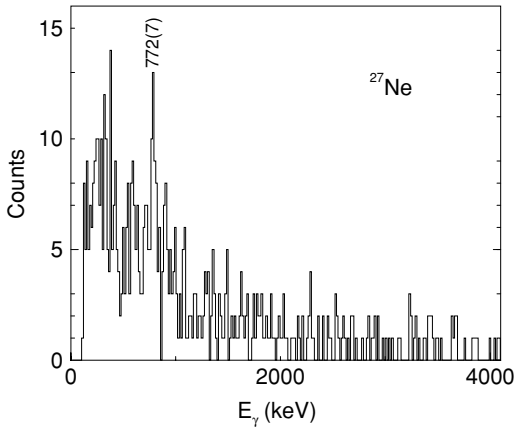

FIG. 4. Ge γ-ray spectrum of ^{27}Ne.

observed in the β-decay of ^{26}F [19], and the latter transition was also seen in a Coulomb excitation experiment [20]. In addition to these lines, several low energy transitions are also visible. These lines are present in the spectra of other isotopes, too, and can be assigned to processes taking place in the laboratory frame as is seen in Fig. 3.

In ^{27}Ne, a single γ-ray peak was observed with relatively low statistics at 772 keV energy. Its existence is confirmed also by the spectrum obtained from the BaF_2 detectors.

For ^{28}Ne, in the spectrum obtained in the double step reaction shown in Fig. 6, three distinct peaks are visible at energies of 914(49), 1314(23), and 1689(38) keV, respectively.

The spectra obtained in the single step reaction are shown in Fig. 5. In the Ge spectrum shown in the inset of Fig. 5, it is clearly seen that a single peak at 1290(9) keV can be associated to ^{28}Ne. In addition to this peak, the known target-like contaminant lines are also visible at about 730 keV. In

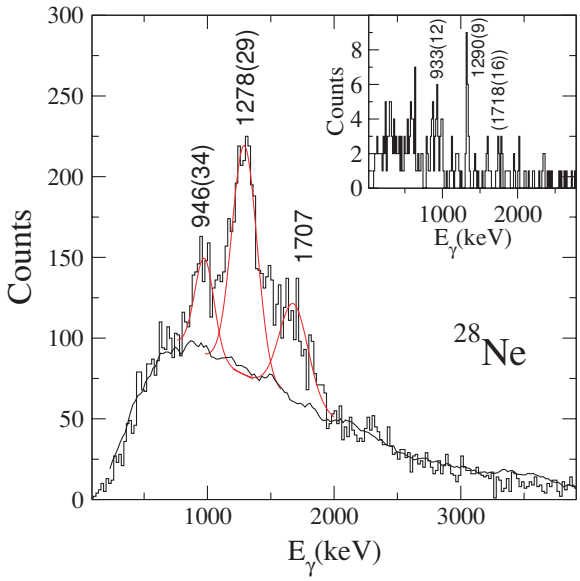

FIG. 5. (Color online) BaF_2 γ-ray spectrum of ^{28}Ne together with a normalized smoothed random background spectrum. In the inset, the γ-spectrum of the Ge detectors is shown.

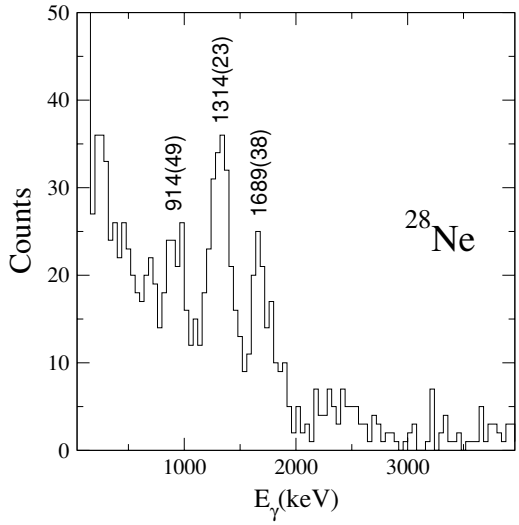

FIG. 6. BaF_2 γ-ray spectrum of ^{28}Ne obtained in the double step fragmentation reaction.

the 850–1050 keV region three close lying peaks are visible. Two of them can be associated to the wide peaks generated by the scattered neutrons in the germanium detector material and shifted by the Doppler correction similarly to the case of ^{26}Ne shown in Fig. 3. The middle line at 933(12) keV can be a γ-line from ^{28}Ne in agreement with the spectrum of the double step reaction. In addition, there is indication for the existence of a weaker line at 1718(16) keV, also in agreement with the results of the double step fragmentation experiment.

In the spectrum of the BaF_2 detectors obtained in the single step reaction a wide, slightly resolved bump of γ-rays can be seen sitting on a relatively large background. To determine the shape of the background below the bump, a background spectrum was generated by setting a gate on the time spectrum very next to the prompt peak for γ-rays and just on the time range corresponding to neutrons. The curve showing the trend

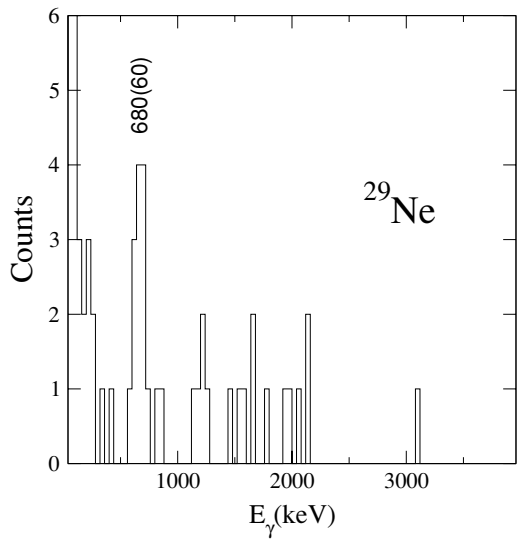

FIG. 7. BaF_2 γ-ray spectrum of ^{29}Ne obtained in the double step fragmentation reaction.

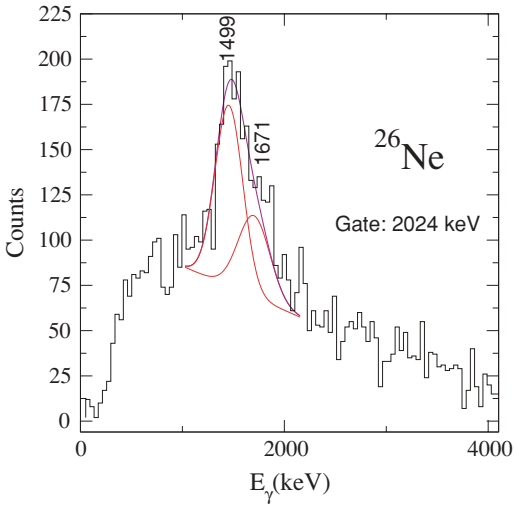

FIG. 8. (Color online) BaF_2 coincidence spectrum of ^{26}Ne gated by the 2024 keV γ-ray.

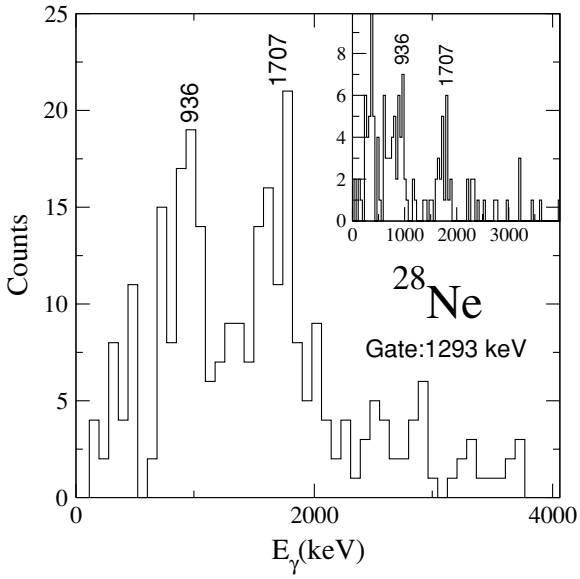

FIG. 9. BaF_2 coincidence spectra of ^{28}Ne gated by the 1289 keV γ-rays obtained in the single-step fragmentation experiment. The spectrum obtained in the double-step experiment is shown in the insert.

of the background in Fig. 5 was produced from the γ-spectrum obtained using the delayed time condition and by normalizing it to the background in the prompt γ-rays spectrum of ^{28}Ne. Knowing the width of peaks from the systematics of single peaks of other nuclei, and fixing the position of the highest energy line, the γ-lines of ^{28}Ne from the single step reaction can also be resolved as it is shown in Fig. 5.

By averaging the energies obtained in the different spectra, we assign 1293(8) keV to the strongest ^{28}Ne γ-ray, 936(28) keV to the lowest energy and 1707(15) keV to the highest energy one. A 1320(20) keV transition has already been observed in Coulomb excitation [20]. A 1319(22) and a 1711(30) keV transition has been also observed in a recent $(p, p\gamma)$ study [21]. In the double step fragmentation experiment a single transition was observed in ^{29}Ne at 680(80) keV energy, which is different from those observed earlier at 450 and 580 keV in the $(p, p\gamma)$ reaction at Riken [3].

From the γ-coincidences obtained from BaF_2 detectors $\gamma\gamma$-matrices have been constructed and analyzed. In ^{26}Ne, putting a narrow gate on the 1499 and 1671 keV lines, it was found that they are in coincidence with the 2024 keV transition. The spectrum gated by the 2024 keV γ-ray is presented in Fig. 8. A wide peak containing the 1499 and the 1671 keV transitions is seen in coincidence with the 2024 keV line.

Despite the low statistics, the spectrum obtained by gating on the 1293 keV line in ^{28}Ne, indicates that the 936 and the 1707 keV γ-rays are in coincidence in Fig. 9, though the statistics is poor. Indications on the coincidence relation between the 1293 and the 936 and 1707 keV lines are present also in the case of the double step fragmentation reaction, as it is shown in the insert of Fig. 9. The result of the coincidence analysis is in accordance with that of the Coulomb excitation measurement, where only a 1320(20) keV transition was observed, suggesting that the other transitions observed in the present study do not feed the ground state directly, but through the 1293(8) keV transition.

Based on the $\gamma\gamma$-coincidence relations as well as on the intensities of the transitions, level schemes were constructed for the nuclei investigated. The level schemes obtained for ^{26}Ne and ^{28}Ne are shown in Figs. 10 and 11, respectively. In ^{27}Ne and ^{29}Ne, we obtained only one excited at 772 keV and 680 keV, respectively.

In ^{26}Ne, the strongest transition with an energy of 2024 keV decays from the first excited state having 2^+ spin-parity in accordance with the β-decay and the Coulomb excitation studies [19,20]. From the β-decay of ^{26}F, an excited state has been proposed at 3691 keV established by the 2018–1673 keV γ-cascade. This assumption is confirmed by our coincidence data. The 1499 keV transition is also in coincidence with the 2024 keV γ-ray and has the second highest intensity, thus, it feeds directly the 2024 keV state.

In ^{28}Ne, the 1293 keV transition has the largest intensity. Therefore, it connects the first excited state of 2^+ spin-parity

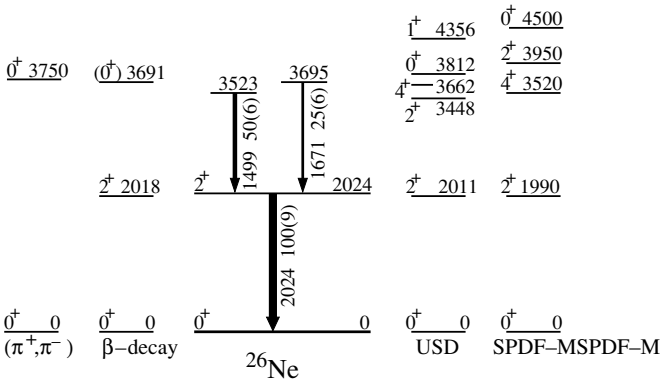

FIG. 10. Proposed level scheme of ^{26}Ne. The results of the shell model calculations with USD and SDPF-M interactions [10,23] are included in the right part of the figure. The previous experimental results are taken from Refs. [19,22].

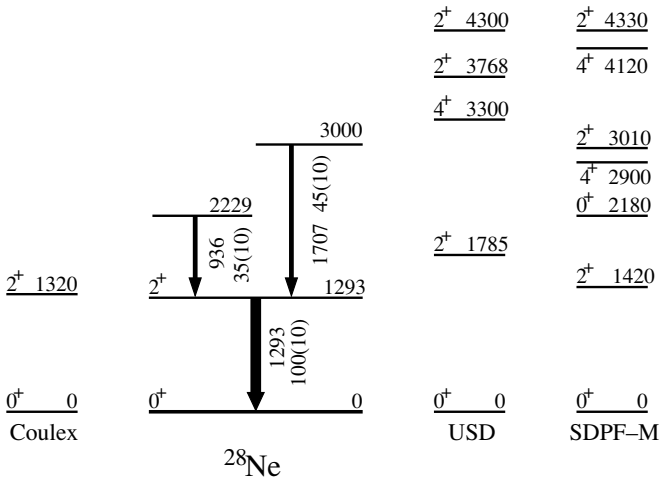

FIG. 11. Proposed level scheme of ^{28}Ne. The results of different shell model calculations [10,23] are included in the right part of the figure. The energy of the first excited state observed in Coulomb excitation experiment is taken from Ref. [20].

and the ground state in agreement with the results of the Coulomb excitation experiment [20]. Based on the coincidence relationships, the 936 and 1531 and 1707 keV transitions correspond to the decay of states above the level at 1293 keV. The 1707 keV transition, observed also in the $(p, p\gamma)$ study, feeds directly the 1293 keV state. The 936 keV transition can be placed either on top of 1293 or the 3000(23) keV states, but from intensity consideration, the former seems to be the more probable.

IV. DISCUSSION

To interpret the experimental results, we compare them with the results of shell calculations. One of the calculations is performed in the *sd* shell using the USD interaction [23]. In the other calculation the model space was extended to include the $p_{3/2}$ and the $f_{7/2}$ orbits from the next major shell, and the effective interaction was changed to the SDPF-M interaction associated with this model space. This interaction was first introduced in Ref. [10] in MCSM calculations, while this name was used later in Ref. [24]. The latter model allows for states generated by neutron excitations across the $N = 20$ shell which may lower to energies observable in the present study even at $N = 16$ or 18. In addition, this model allows the mixing of normal an intruder states, a process which may play a significant role in the structure of nuclei at $N = 18$ [10].

Comparing the experimental level schemes with the results of the shell model calculations, it is seen that some of their features are well described already by the *sd* shell model. In ^{26}Ne, the energy of the 2^+_1 state has the correct energy and the observed two members of the spin 0-2-4 triplet is predicted also well. In the MCSM calculations the 2^+_1 state is at the same position where the USD calculation predicted it, but the triplet becomes more spread, especially the energy of the 0^+_2 state appears at relatively higher energy. Several states are slightly pushed up in energy, partly because of the enlarged $s_{1/2}$-$d_{3/2}$ gap of the SDPF-M interaction. The 2^+_2 state is expected to decay dominantly to the 2^+_1 state, thus it is not possible to distinguish between the 4^+_1 and 2^+_2 states on the basis of their decay properties. According to the MCSM calculations, the 0^+_2 state contains some intruder component, too. The 772 keV energy of the first excited state in ^{27}Ne is rather close to the predicted spin $1/2^+$ state of the USD shell model.

In Fig. 11, one can compare the excited states of ^{28}Ne to the result of the *sd* shell model. The prediction for the 2^+_1 excitation energy (1.8 MeV using the USD interaction) and the experimental result (1.3 MeV) differs more significantly than usual in this model (2–300 keV). This deviation seems to be the consequence of the $N = 20$ shell closure violation proposed by the MCSM calculation [10]. In the *sd* shell model calculations, the second excited state with spin 4 lies at 3.3 MeV, which may correspond to the 3000 keV experimental level. With the parallel placement of the transitions shown in Fig. 11, we are in a complete agreement with the energies predicted by the Monte Carlo shell model calculation. The SDPF-M interaction in MCSM gives the correct 2^+_1 energy and predicts the position of the 0^+_2 state also correctly. Due to the presence of the intruder states, the level density is higher in the MCSM result than that of the *sd* shell model prediction. In the MCSM calculation, the normal and intruder 0^+ states are strongly mixed, and the 2^+_1 state has more intruder component, while the 2^+_2 state is rather a normal one. Similarly, the 4^+_1 state has more intruder component, while the 4^+_2 state has more normal one. It is interesting to mention that some of the previous calculations predict somewhat close value for the 0^+_2 energy to the MCSM, in spite of the different shell gaps used in them.

The difference between the MCSM and other calculations [5,8,9] is not only the shell gap around Ne, but also the treatment of the mixing. The above mentioned calculations do not include mixing between the normal and intruder states. When the mixing is included, the two 0^+ levels repel each other, meaning that a higher energy 0^+_2 level should be obtained in the mixed calculation.

No crossover transition from the experimental state at around 3 MeV to the ground state is observed. This could be an indication for a spin 4 assignment since it might be expected that the 2^+_2 state predicted by the MCSM at 3.0 MeV can decay to various lower lying states, including 2^+_1, with intensities roughly of the same order of magnitude, if the relevant states contain large mixing of intruder configurations. This is not the case, however. In fact, the MCSM result shows that the $E2$ transition from the 2^+_2 state to the ground state is hindered due to the cancellation between proton and neutron contributions, whereas the $M1$ transition from the 2^+_2 to the 2^+_1 states is quite strong. Consequently, the branching ratio is quite large favoring the 2^+_2 to 2^+_1 transition. The above $E2$ hindrance and $M1$ enhancement are consequences of an isovector excitation character of the 2^+_2 state. This feature is seen also in the *sd* shell model, but is strengthened by a factor of 2.6 due to the mixing of intruder configurations.

The proposed level scheme for ^{28}Ne is fully consistent with the MCSM calculations and the observation of the excited state at 2229 keV can only be interpreted by the assumption of neutron excitation across the $N = 20$ shell. In a naive shell

model this state can be assigned to the 0^+ state intruding from the *fp* shell, but in MCSM its low energy provokes a mixing of the normal and the intruder configurations resulting also in lowering of the energy of the 2_1^+ state. The need for excitations across the $N = 20$ shell gap is also supported by the observation of low energy states in ^{29}Ne, where the *sd* shell model predicts the first excited state at about 1.9 MeV. At least some of them can be interpreted as one-particle–two-hole excitations across the $N = 20$ shell gap.

V. SUMMARY

Summarizing our results, we have studied the structure of $^{25-29}$Ne by use of in-beam γ-ray spectroscopy with projectile fragmentation reactions. We have established a new state at about 3.5 MeV in ^{26}Ne, a bound excited state in ^{27}Ne as well as in ^{29}Ne, and new excited states are proposed in ^{28}Ne. The major part of the experimental data is consistent with both the *sd* and the Monte Carlo shell model calculations. However, observation of extra states relative to the *sd* shell model prediction in ^{28}Ne and ^{29}Ne clearly indicate the presence of neutron cross shell excitation already at $N = 18, 19$ in Ne isotopes. These observations are supported by a recent study of ^{29}Na, where the the need for neutron cross shell excitations was also claimed [25].

ACKNOWLEDGMENTS

This work has been partially supported by the European Community Contract No. HPRI-CT-1999-00019, and also by OTKA T38404, T42733, T46901, PICS(IN2P3) 1171, INTAS 00-00463, GACR 202-04791 and RFBR N96-02-17381a grants, by the Bolyai János Foundation, as well as by Grant-in-Aid for Specially Promoted Research (13002001) from MEXT, and by the RIKEN-CNS collaboration project on large-scale nuclear structure calculation.

[1] C. Detraz, D. Guillemaud, G. Huber, R. Klapisch, M. Langevin, F. Naulin, C. Thibault, L. C. Carraz, and F. Touchard, Phys. Rev. C **19**, 164 (1978).
[2] G. Klotz, P. Baumann, M. Bounajma, A. Huck, A. Knipper, G. Walter, G. Marguier, C. Richard-Serre, A. Poves, and J. Retamosa, Phys. Rev. C **47**, 2502 (1993).
[3] Y. Yanagisawa *et al*., Phys. Lett. **B566**, 84 (2003).
[4] F. Azaiez *et al*., Phys. Scr. T **88**, 118 (2000).
[5] E. K. Warburton, J. A. Becker, and B. A. Brown, Phys. Rev. C **41**, 1147 (1990).
[6] N. Fukunishi, T. Otsuka, and T. Sebe, Phys. Lett. **B296**, 279 (1992).
[7] T. Siiskonen, P. O. Lipas, and J. Rikovska, Phys. Rev. C **60**, 034312 (1999).
[8] E. Caurier, F. Nowacki, A. Poves, and J. Retamosa, Phys. Rev. C **58**, 2033 (1998).
[9] E. Caurier *et al*., Nucl. Phys. **A693**, 374 (2001).
[10] Y. Utsuno, T. Otsuka, T. Mizusaki, and M. Honma, Phys. Rev. C **60**, 054315 (1999).
[11] T. Otsuka, R. Fujimoto, Y. Utsuno, B. A. Brown, M. Honma, and T. Mizusaki, Phys. Rev. Lett. **87**, 082502 (2001).
[12] M.-J. Lopez-Jimenez, Ph.D. thesis, GANIL T 00 01, Ganil, Caen, 2000.
[13] M. Belleguic-Pigeard de Gurbert, Ph.D. thesis, IPNO-T-00-05, Institute de Physique Nucleaire, Orsay, 2000.
[14] D. Sohler *et al*., Phys. Rev. C **66**, 054302 (2002).
[15] O. Sorlin *et al*., Eur. Phys. J. A **22**, 173 (2004).
[16] Z. Dombrádi *et al*., Nucl. Phys. **A727**, 195 (2003).
[17] M. Stanoiu *et al*., Phys. Rev. C **69**, 034312 (2004).
[18] L. Bianchi *et al*., Nucl. Instrum. Methods Phys. Res. A **276**, 509 (1989).
[19] A. T. Reed *et al*., Phys. Rev. C **60**, 024311 (1999).
[20] B. V. Pritychenko *et al*., Phys. Lett. **B461**, 322 (1999).
[21] Z. Elekes *et al*., Eur. Phys. J. A, accepted for publication.
[22] H. Nann, K. K. Seth, S. G. Iversen, M. O. Kaletka, D. B. Barlow, and D. Smith, Phys. Lett. **B96**, 261 (1980).
[23] B. H. Wildenthal, Prog. Part. Nucl. Phys. **11**, 5 (1984).
[24] Y. Utsuno, T. Otsuka, T. Glasmacher, T. Mizusaki, and M. Honma, Phys. Rev. C **70**, 044307 (2004).
[25] V. Tripathi *et al*., Phys. Rev. Lett. **94**, 162501 (2005).